

# Reconstruction of sectional images in holography using inverse imaging

Xin Zhang,<sup>1</sup> Edmund Y. Lam,<sup>1,\*</sup> and Ting-Chung Poon<sup>2</sup>

<sup>1</sup>*Imaging Systems Laboratory,  
Department of Electrical and Electronic Engineering,  
The University of Hong Kong, Pokfulam Road, Hong Kong*

<sup>2</sup>*Bradley Department of Electrical and Computer Engineering,  
Virginia Polytechnic Institute and State University,  
Blacksburg, Virginia 24061, USA*

[elam@eee.hku.hk](mailto:elam@eee.hku.hk)

**Abstract:** This paper discusses the reconstruction of sectional images from a hologram generated by optical scanning holography. We present a mathematical model for the holographic image capture, which facilitates the use of inverse imaging techniques to recover individual sections. This framework is much more flexible than existing work, in the sense that it can handle objects with multiple sections, and possibly corrupted with white Gaussian noise. Simulation results show that the algorithm is capable of recovering a prescribed section while suppressing the other ones as defocus noise. The proposed algorithm is applicable to on-axis holograms acquired by conventional holography as well as phase-shifting holography.

© 2008 Optical Society of America

**OCIS codes:** (090.1760) Computer holography; (180.6900) Three-dimensional microscopy; (100.3190) Inverse problems; (100.3020) Image reconstruction-restoration; (110.1758) Computational imaging.

---

## References and links

1. B. D. Duncan and T.-C. Poon, "Gaussian Beam Analysis of Optical Scanning Holography," *J. Opt. Soc. Am. A* **9**, 229–236 (1992).
2. B. W. Schilling and G. C. Templeton, "Three-dimensional Remote Sensing by Optical Scanning Holography," *Applied Optics* **40**, 5474–5481 (2001).
3. T. Kim, T.-C. Poon, and G. Indebetouw, "Depth Detection and Image Recovery in Remote Sensing by Optical Scanning Holography," *Opt. Eng.* **41**, 1331–1338 (2002).
4. P. P. Banerjee and R. M. Misra, "Dependence of Photorefractive Beam Fanning on Beam Parameters," *Optics Communications* **100**, 166–172 (1993).
5. T.-C. Poon, "Recent Progress in Optical Scanning Holography," *J. Holography Speckle* **1**, 6–25 (2004).
6. G. Indebetouw and W. Zhong, "Scanning Holographic Microscopy of Three-dimensional Fluorescent Specimens," *J. Opt. Soc. Am. A* **23**, 1699–1707 (2006).
7. T.-C. Poon, "Scanning Holography and Two-dimensional Image Processing by Acousto-optic Two-pupil Synthesis," *J. Opt. Soc. Am. A* **2**, 521–527 (1985).
8. C. J. Kuo, "Electronic Holography," *Opt. Eng.* **35**, 1528 (1996).
9. K. M. Johnson, M. Armstrong, L. Hesselink, and J. W. Goodman, "Multiple Multiple-exposure Hologram," *Applied Optics* **24**, 4467–4472 (1985).
10. G. Indebetouw, "Properties of a Scanning Holographic Microscopy: Improved Resolution, Extended Depth-of-focus, and/or Optical Sectioning," *J. Mod. Opt.* **49**, 1479–1500 (2002).
11. T. Kim, "Optical Sectioning by Optical Scanning Holography and a Wiener Filter," *Applied Optics* **45**, 872–879 (2006).
12. H. Kim, S.-W. Min, B. Lee, and T.-C. Poon, "Optical Sectioning for Optical Scanning Holography Using Phase-space Filtering with Wigner Distribution Functions," *Applied Optics* **47**, 164–175 (2008).

13. H. M. Ozaktas, Z. Zalevsky, and M. A. Kutay, *The Fractional Fourier Transform: with Applications in Optics and Signal Processing*, 1st ed. (Wiley, Chichester, 2001).
  14. T.-C. Poon, *Optical Scanning Holography with MATLAB*, 1st ed. (Springer-Verlag, New York, 2007).
  15. J. Swoger, M. Martínez-Corral, J. Huisken, and E. Stelzer, "Optical Scanning Holography as a Technique for High-resolution Three-dimensional Biological Microscopy," *J. Opt. Soc. Am. A* **19**, 1910–1918 (2002).
  16. G. Indebetouw, W. Zhong, and D. Chamberlin-Long, "Point-spread Function Synthesis in Scanning Holographic Microscopy," *J. Opt. Soc. Am. A* **23**, 1708–1717 (2006).
  17. M. R. Banham and A. K. Katsaggelos, "Digital Image Restoration," *IEEE Signal Processing Magazine* **14**, 24–41 (1997).
  18. J. M. Blackledge, *Digital Image Processing: Mathematical and Computational Methods*, 1st ed. (Horwood, West Sussex, 2005).
  19. A. Tikhonov and V. Arsenin, *Solutions of Ill-posed Problems*, 1st ed. (V.H. Winston and Sons, Washington, 1977).
  20. F. Natterer and F. Wübbeling, *Mathematical Methods in Image Reconstruction*, 1st ed. (SIAM, Philadelphia, 2001).
  21. L. Vese, "A Study in the BV Space of a Denoising-deblurring Variational Problem," *Applied Mathematics and Optimization* **44**, 131–161 (2001).
  22. G. Aubert and P. Kornprobst, *Mathematical Problems in Image Processing: Partial Differential Equations and Calculus of Variations*, 2nd ed. (Springer-Verlag, New York, 2006).
  23. C. R. Vogel, *Computational Methods for Inverse Problems*, 1st ed. (SIAM, Philadelphia, 2002).
- 

## 1. Introduction

Optical scanning holography (OSH) is a technique which records the holographic information of a three-dimensional (3-D) object on a two-dimensional (2-D) hologram by lateral scanning [1]. Nowadays, it covers a great number of application areas, such as holographic fluorescence microscopy, remote sensing and biological microscopy [2, 3, 4, 5, 6]. The first system was designed by Poon in 1985 [7]. It is a two-pupil system, in which two coherent beams illuminate a point pupil and a uniform pupil, respectively [7]. They are then combined to take a raster scan over an object, and the holographic information is captured to form electronic holograms [8].

Using optical scanning, multiple sections of an object are recorded on a 2-D hologram [9]. Generally, the hologram is complex-valued and contains information from all sections. The technique is advantageous as the hologram contains volume information of the 3-D object being scanned. However, the challenge is with the reconstruction of individual sections from the hologram. The major reason lies in the suppression of defocus noise [10]. From a hologram containing two or more sectional images to be reconstructed, when one intends to retrieve a section, the other sections will manifest as defocus images, which we treat as noise with regard to the in-focus section. The more sections a hologram contains, the more serious the defocus noise appears. Therefore, the suppression of defocus noise is mandatory in the reconstruction of sectional images from a hologram.

The conventional method to obtain sectional images in OSH involves computing the convolution of the hologram with the conjugate impulse response at the focused position. This convolution operation extracts the focus image but the image is contaminated with interferences from other defocused sectional images. Two recent methods were developed particularly to reduce the visibility of the defocus images. Kim [11] proposed to reconstruct sectional images by means of a Wiener filter, which is an optimal filter, in a statistical sense, widely used in image restoration. The method was shown to outperform the conventional technique described above. However, the Wiener filter is optimal provided we can get accurate measurement of the power spectral density. When the intensity distribution of a section is quite similar to the other, the estimator is biased greatly from the true noise, so that results would be less meaningful. In addition, it seems to work only with two sections, and with virtually no noise in the imaging system. More recently, Wigner distribution function (WDF) is also used in the reconstruction of sectional images [12]. The method takes advantage of the relationship between fractional

Fourier transform and WDF to distinguish the information of sectional images [13]. Yet, for an image the Wigner distribution is a 4-D function, and the image reconstruction is thus computationally intensive. Furthermore, both methods described above have only been demonstrated for two sections. With more sections, the interference among those sections in a hologram is larger, resulting in more pronounced defocus noise.

In this paper, our goal is to design a flexible image reconstruction technique that can obtain sectional images from OSH. Our method requires only a moderate computational load typical of image reconstruction techniques, can handle multiple sections, and incorporates noise in the imaging model. We achieve this by formulating the imaging using a matrix approach, resulting in an inverse imaging problem for the sectioning of the hologram. To cope with the ill-posed nature of the imaging, regularization is used, together with an iterative approach using conjugate gradient (CG) for the successive computations.

This paper is structured as follows. In Section 2, we describe the basic principles of the OSH system and introduce the mathematical model we use for the imaging. A hologram containing two sections is described as an example. In Section 3, the regularization technique and implementation using iterative techniques are presented. Section 4 shows the results of two experiments on two- and three-sectional images resulting from holograms. Finally, Section 5 concludes this paper.

## 2. Imaging Model

### 2.1. Principles of Optical Scanning Holography

Optical Scanning Holography (OSH) records the holographic information of a 3-D object by optical heterodyne scanning. Its schematic is shown in Fig. 1, which was first analyzed by Poon in 1985 [7]. In the system, two coherent beams of different temporal frequencies  $\omega + \alpha$  and  $\omega$  pass through two pupils  $p_1$  and  $p_2$  respectively, and they are then combined together by a beam

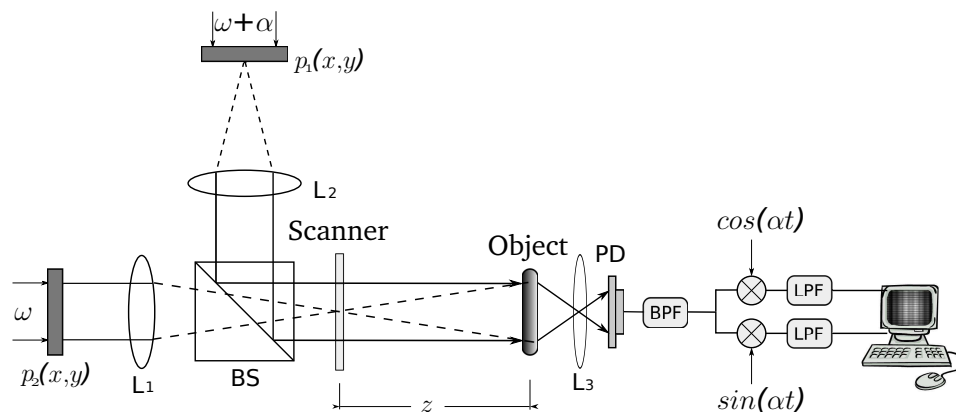


Fig. 1. A typical double-beam optical scanning holography system.

splitter (BS). The combined beam is projected onto a section of an object, which is at a distance  $z$  away from the scanner in the system. A photodetector (PD) collects transmitted and scattered light from the object and converts it to an electronic signal. The demodulation part that follows, including a bandpass filter (BPF) centred at frequency  $\alpha$ , an electronic multiplexing detection and low pass filters (LPF), processes the signal and generates two electronic holograms in a computer.

Mathematical analysis of the OSH system has been conducted by Poon [14] and Swoger et al. [15] in details. Its optical transfer function (OTF) is

$$H(k_x, k_y; z)|_{\text{osh}} = \exp \left\{ -j \frac{z}{2k_0} (k_x^2 + k_y^2) \right\}, \quad (1)$$

where  $k_0$  is a constant and  $z$  is the distance as shown in Fig. 1. The corresponding spatial impulse response is

$$h(x, y; z)|_{\text{osh}} = -j \frac{k_0}{2\pi z} \exp \left\{ \frac{jk_0(x^2 + y^2)}{2z} \right\}. \quad (2)$$

Given an object with complex amplitude expressed by  $\phi(x, y; z)$ , its complex hologram by OSH in an incoherent mode of operation is given by

$$g_c(x, y) = \int_{-\infty}^{\infty} \{ |\phi(x, y; z)|^2 * h(x, y; z) \} dz, \quad (3)$$

where  $*$  denotes the convolution operation. For discretized sectional images,  $z$  can be denoted by  $z_1, z_2, \dots, z_n$ . Then, the hologram can be represented by a summation,

$$g_c(x, y) = \sum_{i=1}^n \{ |\phi(x, y; z_i)|^2 * h(x, y; z_i) \}. \quad (4)$$

Suppose the focused plane is located at  $z_1$ . A reconstruction of this sectional image means to recover  $|\phi(x, y, z_1)|^2$  from a hologram  $g_c(x, y)$ .

## 2.2. Two-Sectional Images: An Example

$g_c(x, y)$  in Eq. (4) is a general expression with  $n$  sections. As mentioned above, the current literature has demonstrated methods only with two-sectional images. In what follows, we set  $n = 2$  to simplify the description, but we note here that generalizing to other values of  $n$  is straightforward and is done for the simulation with three sections.

When an object has only two sections, Eq. (4) can be simplified to

$$g_c(x, y) = |\phi(x, y; z_1)|^2 * h(x, y; z_1) + |\phi(x, y; z_2)|^2 * h(x, y; z_2). \quad (5)$$

Because OSH is a linear space-invariant system [16], we can use the convolution operation to formulate a hologram. The hologram by heterodyne scanning technique is recorded in the digital form, i.e., a matrix in a computer, which contains samples of the function  $g_c(x, y)$ .

It is possible to express the convolution in terms of matrix multiplication. Let

$$h_1(x, y) = h(x, y; z_1) = -j \frac{k_0}{2\pi z_1} \exp \left\{ \frac{jk_0(x^2 + y^2)}{2z_1} \right\}, \quad (6)$$

$$h_2(x, y) = h(x, y; z_2) = -j \frac{k_0}{2\pi z_2} \exp \left\{ \frac{jk_0(x^2 + y^2)}{2z_2} \right\}. \quad (7)$$

The convolution with  $h_1(x, y)$  and  $h_2(x, y)$  can be expressed as follows. First, we use a lexicographical ordering to convert  $|\phi(x, y; z_1)|^2$  and  $|\phi(x, y; z_2)|^2$  into vectors, which we denote as  $\psi_1$  and  $\psi_2$  respectively. If the original hologram is of size  $N \times N$ , then these vectors are of a length  $N^2$ . Similarly, we also convert  $g_c(x, y)$  into the length- $N^2$  vector, which we call  $\gamma_c$ . We then form two  $N^2 \times N^2$  matrices,  $H_1$  and  $H_2$ , using values from  $h_1(x, y)$  and  $h_2(x, y)$  respectively, so that Eq. (5) becomes

$$\gamma_c = H_1 \psi_1 + H_2 \psi_2. \quad (8)$$

Note that both  $H_1$  and  $H_2$  are block-circulant-circulant-block (BCCB) if we assume periodic extension on the boundary [17], which would be easiest for an implementation using fast Fourier transform.

We can simplify Eq. (8) further by writing

$$\gamma_c = \begin{bmatrix} H_1 & H_2 \end{bmatrix} \begin{bmatrix} \psi_1 \\ \psi_2 \end{bmatrix} = H\psi, \quad (9)$$

where  $H = \begin{bmatrix} H_1 & H_2 \end{bmatrix}$  and  $\psi = \begin{bmatrix} \psi_1^T & \psi_2^T \end{bmatrix}^T$ . Note that  $H$  is the matrix representing the operation in OSH, which scans an object denoted by  $\psi$ , and generates  $\gamma_c$ . To reconstruct sectional images from a hologram, we need to compute  $\psi$  from the observed  $\gamma_c$ , which is an inverse imaging problem.

We remark here that the relationship  $\gamma_c = H\psi$  is also applicable to multiple sections in OSH, provided we let  $H = \begin{bmatrix} H_1 & \cdots & H_n \end{bmatrix}$  and  $\psi = \begin{bmatrix} \psi_1^T & \cdots & \psi_n^T \end{bmatrix}^T$ . Thus, the inverse imaging approach is applicable to more than two sections, which goes beyond the methods described in [11, 12].

### 3. Computational Considerations

$H$  and  $\gamma_c$  in Eq. (9) are complex-valued in general. It is however possible to work on real-valued quantities, by first pre-processing the signals similar to the conventional reconstruction method. This also allows us to eliminate the imaginary part of the defocus noise.

Suppose we intend to focus on the section at  $z_1$ . From Eq. (5), we can convolve both sides with the complex conjugate free-space impulse response  $h_1(x, y)$ , somewhat like a matched filter. Thus,

$$\begin{aligned} g_c(x, y) * h_1^*(x, y) &= |\phi(x, y; z_1)|^2 * h_1(x, y) * h_1^*(x, y) + |\phi(x, y; z_2)|^2 * h_2(x, y) * h_1^*(x, y) \\ &= |\phi(x, y; z_1)|^2 + |\phi(x, y; z_2)|^2 * h_{21}(x, y), \end{aligned} \quad (10)$$

where

$$\begin{aligned} h_1(x, y) * h_1^*(x, y) &\approx \delta(x, y) \text{ (except scaling);} \\ h_2(x, y) * h_1^*(x, y) &= h(x, y; z_2 - z_1) = h_{21}(x, y). \end{aligned} \quad (11)$$

The second term  $|\phi(x, y; z_2)|^2 * h_{21}(x, y)$  in Eq. (10) is the defocus noise imposed on the focused section at  $z_1$ . It should be noted that the convolution with the conjugate impulse response  $h_1^*(x, y)$  keeps the focused section purely real and the defocused section complex. Then we separate out the imaginary part of the defocused section by preserving the real-valued part of  $g_c(x, y) * h_1^*(x, y)$ .

Using matrix notation similar to that in Eq. (9), we are essentially computing

$$H_1^* \gamma_c = H_1^* H \psi. \quad (12)$$

By retaining the real part of both sides of the equation only, we can eliminate the imaginary part of the defocus noise completely. Since  $\psi$  is real, the imaging equation becomes

$$\text{Re}[H_1^* \gamma_c] = \text{Re}[H_1^* H] \psi, \quad (13)$$

where  $\text{Re}[\cdot]$  means taking the real part of a complex quantity. Let  $\beta_c = \text{Re}[H_1^* \gamma_c]$  and  $A = \text{Re}[H_1^* H]$ . The inverse imaging equation we will solve is

$$\beta_c = A\psi + v, \quad (14)$$

where we also add the term  $v$  above to denote random Gaussian noise that is present in a typical imaging system.

We can only find an approximation of  $\psi$  in the equation above because of the ill-posed nature of the inverse imaging problem [18]. The regularization method is employed to reach the solution [19]. We formulate the image reconstruction as a minimization problem [20]:

$$f(\psi) = \|A\psi - \beta_c\|^2 + \lambda \|C\psi\|^2, \quad (15)$$

where  $\|\cdot\|$  denotes the  $L^2$  norm,  $C$  stands for the Laplacian operator, and  $\lambda$  is the regularization parameter. The first term  $\|A\psi - \beta_c\|^2$  measures the fidelity of  $\psi$  to the observed data  $\beta_c$ , and the second term  $\|C\psi\|^2$  is a penalty arising from the prior knowledge of  $\psi$ . Since sectional images of a hologram present the same characteristic of smoothness as common images,  $C$  is chosen as a high pass filter to suppress noise at higher frequencies.

The regularized minimization problem has been well studied in terms of the existence and uniqueness of a solution [21, 22]. Generally, in implementation,  $A$  and  $C$  matrices are either huge or rank deficient, or both. We use the CG method to solve the set of linear equations, which has a symmetric positive definite coefficient matrix,  $A^T A + \lambda C^T C$ , for  $\lambda > 0$  [23]. The  $k$ th step of the CG process takes the form  $\psi^{(k)} = \psi^{(k-1)} + a_k p^{(k)}$ , where

$$\begin{aligned} b_k &= \frac{\|q^{(k-1)}\|^2}{\|q^{(k-2)}\|^2} \\ p^{(k)} &= q^{(k-1)} + b_k p^{(k-1)} \\ a_k &= \frac{\|q^{(k-1)}\|^2}{\|(A^T A + \lambda C^T C)p^{(k)}\|^2} \\ q^{(k)} &= q^{(k-1)} - a_k (A^T A + \lambda C^T C)p^{(k)}. \end{aligned} \quad (16)$$

$\psi^{(k)}$  is the approximation to  $\psi$  after  $k$  iterations, and  $p^{(k)}$  and  $q^{(k)}$  are two auxiliary iteration vectors of length  $n^2$ .

## 4. Results

Two experiments are conducted to demonstrate the performance of the proposed methodology on the reconstruction of sectional images encoded in a hologram. The first one aims to investigate its capability of suppressing white Gaussian noise and overcoming the influence of defocus noise. The second one is designed to verify that the methodology is generally applicable to a hologram with multiple sections. Note that these are computer simulations, in line with [11, 12] which also demonstrate their algorithms on such synthetic experiments.

### 4.1. Hologram Containing 2-sectional Images

The first experiment is performed on an object drawn in Fig. 2(a) and contains two elements in two distinct sections,  $z_1$  and  $z_2$ , away from the scanner of the OSH system. We suppose that the object is illuminated by a HeNe laser, whose wavelength is  $0.63\mu\text{m}$ , and that two sections including an element in each are located at  $z_1 = 10\text{mm}$  and  $z_2 = 11\text{mm}$ , respectively. The two sections are scanned to generate a hologram. During the scanning, the hologram is contaminated by additive white Gaussian noise with zero mean and variance of 0.01.

Fresnel zone plates (FZPs) of a point source at  $z_1$  and  $z_2$  are shown in Fig. 2(b). The spatial rate of change in the phase varies along  $x$  and  $y$  directions. The rate at which the FZP varies is determined by the distance between the focus of  $L_1$  and the plane to be reconstructed in the object. The shorter the distance is, the higher rate the FZP varies at. Optical scanning technique

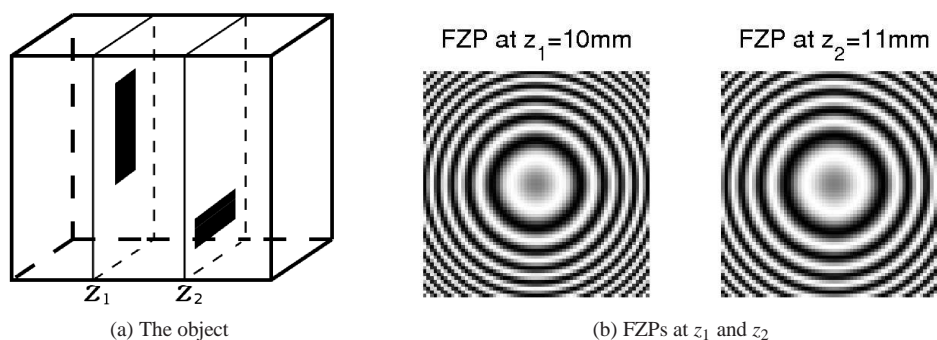


Fig. 2. The object and FZPs in the first experiment. Shown in Fig. 2(a) is the object, in which two elements (i.e., rectangles) are at  $z_1$  and  $z_2$  sections, respectively. Shown in Fig. 2(b) are the real parts of FZPs of a point source at  $z_1$  and  $z_2$ .

produces the complex hologram of the object. The real part of the hologram is referred to as the sine-FZP hologram, while the imaginary part is the cosine-FZP hologram [14]. Fig. 3 presents the two kinds of holograms. Visually, it is hard to figure out any intensity distribution information of the two sections. To obtain the information of the sections from the complex hologram,

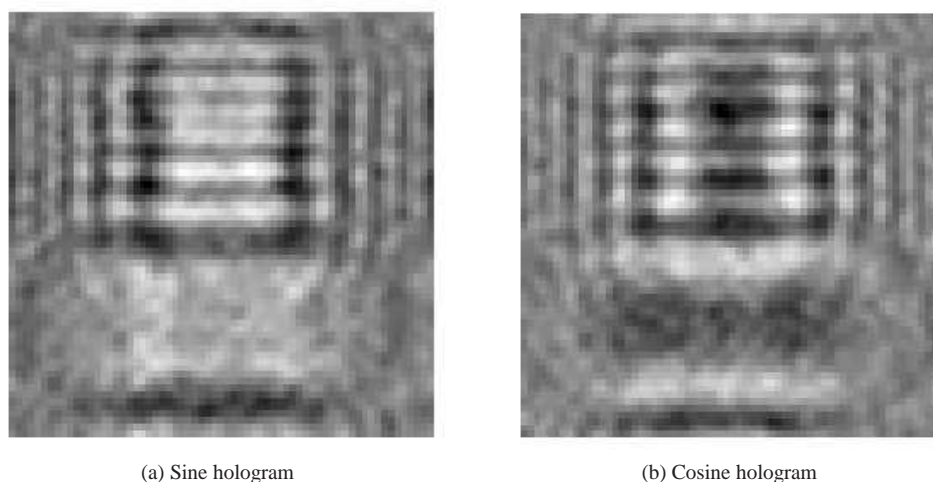


Fig. 3. The holograms containing two-sectional images of the object in the first experiment

the reconstruction methods discussed above are implemented. Among them, the conventional method is straightforward. It makes use of Eq. (10) only, without taking into consideration the regularization in inverse imaging. Results by this method are shown in Fig. 4, in which Fig. 4(a) corresponds to the reconstructed section at  $z_1$ , and Fig. 4(b) to the one at  $z_2$ . Relating them with the two original sections of the object in Fig. 2(a), the rectangular elements are recovered in the corresponding focused sections, and the defocus noise is weakened at the same time. The weakening effect results from the preservation of real-valued part, which eliminates the imaginary part of the defocus noise. However, we observe blurry residuals due to the remaining real part of the defocus noise.

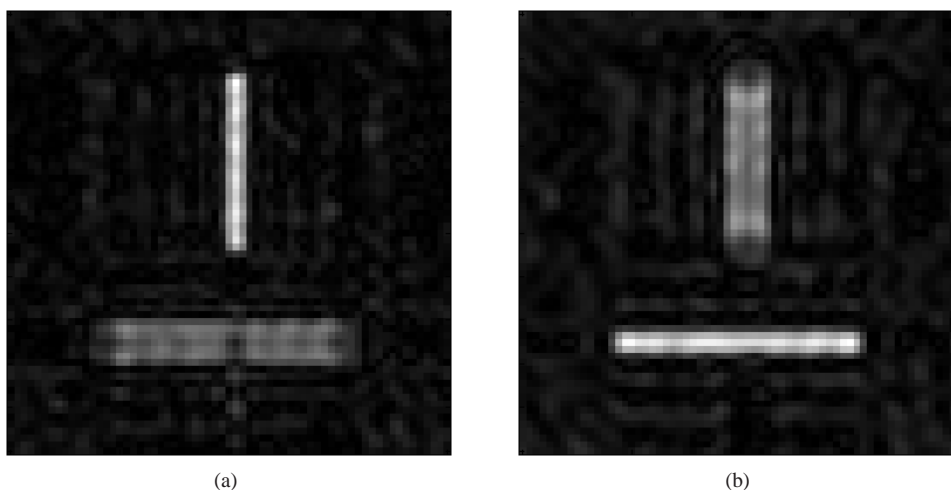


Fig. 4. Reconstructed sections by the conventional method on the hologram containing two sections only. Fig. 4(a) is the result of  $z_1$  section and Fig. 4(b) is that of  $z_2$  section.

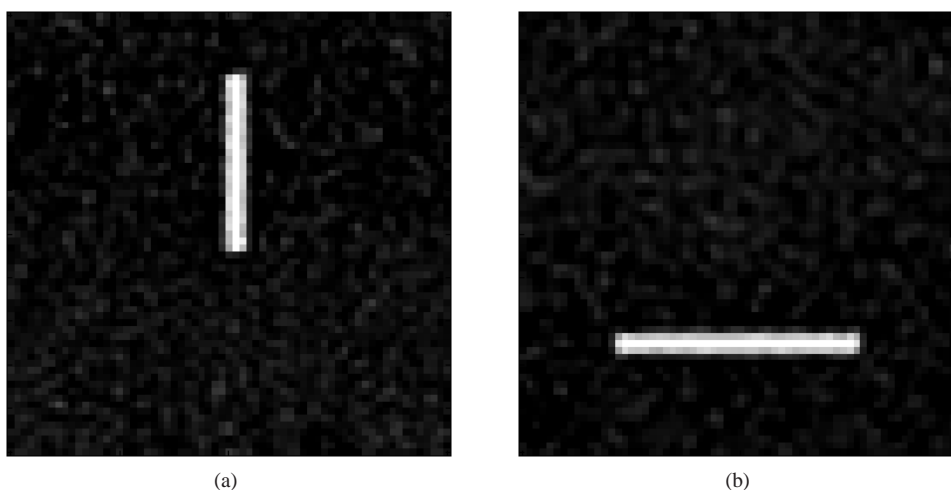


Fig. 5. Reconstructed sections by the inverse imaging method from the hologram with two sections. Fig. 5(a) is reconstructed section at  $z_1$  and Fig. 5(b) is the one at  $z_2$ .

In comparison, the inverse imaging method is used to reconstruct the sectional images and suppress the defocus noise. The reconstructed images are shown in Fig. 5. As shown, each reconstructed section is only mildly influenced by the defocus noise, and the element in each is clearly recovered. Signal-to-noise ratio (SNR) between the original sections and the recovered ones is 29.93 dB at  $z_1$  and 28.85 dB at  $z_2$ . Since our algorithm is iterative in nature, a stopping criterion is needed. Our experience through various experiments is that the total number of iterations is effective as a simple rule, with around 50 iterations sufficient to obtain an acceptable reconstruction. Since the core of our algorithm is conjugate gradient, which is frequently employed in image processing, it can be expected that this would not induce a heavy computation



in a reasonable implementation. It is also possible to take advantage of the structure of the  $H$  matrix in Eq. (9) to improve the speed of the algorithm. The experiment demonstrates that the reconstruction can recover sectional images without visible influence of defocus noise, and with efficient suppression of additive white Gaussian noise.

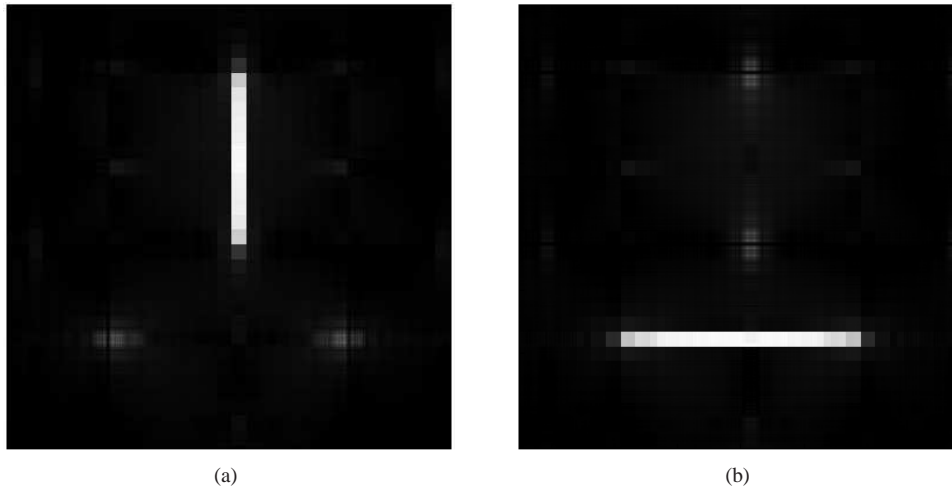


Fig. 6. Reconstructed sections by Wiener filter. Fig. 6(a) is reconstructed section at  $z_1$  and Fig. 6(b) is the one at  $z_2$ .

To show the advantages of our reconstruction method, a comparison is also conducted to consider results from Wiener filter and WDF using a two-section object. We apply the Wiener filter to the same object as we use above, but without additive noise. Reconstructed sectional images are shown in Fig. 6. Defocus noise in each section appears significantly suppressed. Central parts of the defocus element are filtered out, and terminal points are weakened to the extent that only gray parts are left. Wiener filter achieves the reconstruction with a sufficient suppression of the defocus noise. While this is useful, it should be noted that it requires an *a priori* knowledge of the power spectrum of the noise. Here, the spectrum is estimated by the imaginary part of the defocus noise. The method is suitable for objects containing elements with regular density distributions. To those including either complicated elements or multiple sections, the imaginary part is comprised of the information of various elements. The error of the estimator increases significantly, and the reconstruction can become complicated and error-prone.

To investigate the reconstruction by WDF, we analyze the same object as used in the work by Kim *et al.* [12], which proposed to adopt WDF and gave a detailed description about the application of WDF to the reconstruction. Interested readers can refer to this publication for details regarding its computation. In brief, the two sections are represented by two components with certain rotations in the space-frequency domain. A large difference between the rotation degrees implies a high possibility of separating them. This depends on the distance between the two sections. Moreover, because WDF contains the interference terms, the degrees of the geometric rotation are required to be different enough to effectively decrease these unwanted terms. Accordingly, WDF has only been shown to work on simple two-section objects, such as parallel bars that are spaced rather far apart. We attempted to apply this technique to our scenario depicted in Fig. 2, but the computational burden (since the WDF of a general 2D signal is a 4D distribution) renders that not possible at the moment.

#### 4.2. Hologram Containing 3-sectional Images

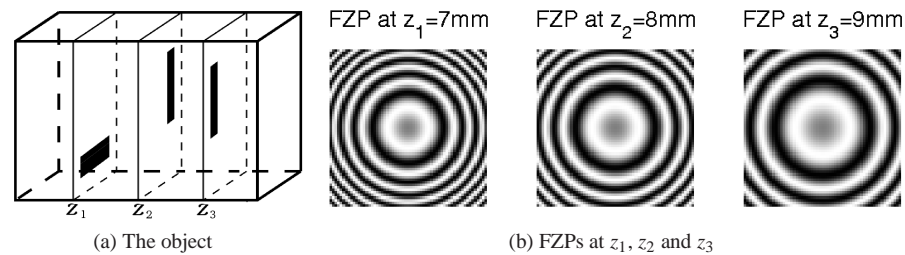


Fig. 7. The object and FZPs in the three-section experiment. The object in Fig. 7(a) contains three elements at  $z_1 = 7\text{mm}$ ,  $z_2 = 8\text{mm}$  and  $z_3 = 9\text{mm}$  sections. Real parts of FZPs of a point source at  $z_1$ ,  $z_2$  and  $z_3$  are shown in Fig. 7(b).

The next experiment is intended to demonstrate the reconstruction by the inverse imaging on multiple sections. It is computed on an object with three elements locating at  $z_1$ ,  $z_2$  and  $z_3$  sections. They are shown in Fig. 7(a). The object is scanned by the same laser as used in the first experiment. Three sections are  $z_1 = 7\text{mm}$ ,  $z_2 = 8\text{mm}$  and  $z_3 = 9\text{mm}$  away from the scanner. White Gaussian noise corrupts the hologram, with a resulting SNR equal to 28 dB. FZPs of a point source in three section are shown in Fig. 7(b). The noisy hologram is shown in Fig. 8. It combines the sectional images at  $z_1$ ,  $z_2$  and  $z_3$  together. The hologram is more mixed than a

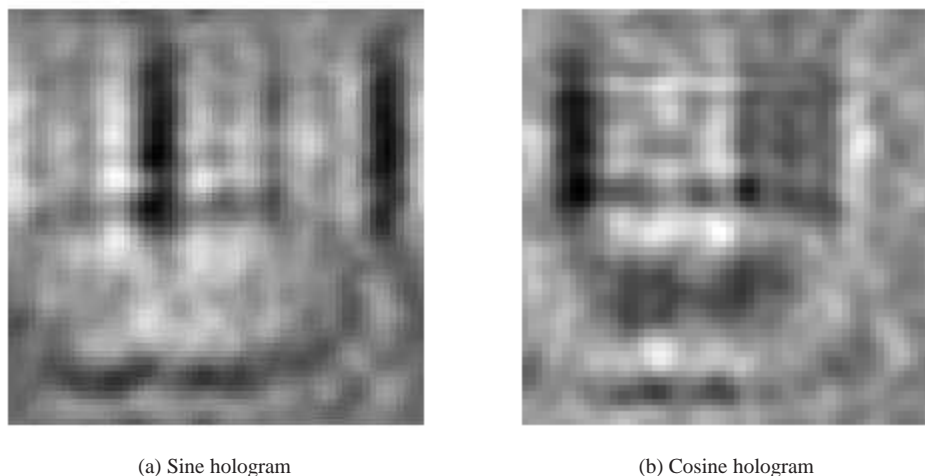


Fig. 8. The hologram containing three-sectional images of the object in the second experiment

two-section hologram and consequently it is more difficult to acquire any sectional information by reviewing it directly.

The conventional and the inverse imaging method are implemented to recover the sectional information of the hologram successively. Shown in Fig. 9 are reconstructed sectional images. Results from the conventional method are displayed in Fig. 9(a), Fig. 9(b) and Fig. 9(c). We can see rather substantial presence of noise. Gray and blurry defocus noise is impressive and

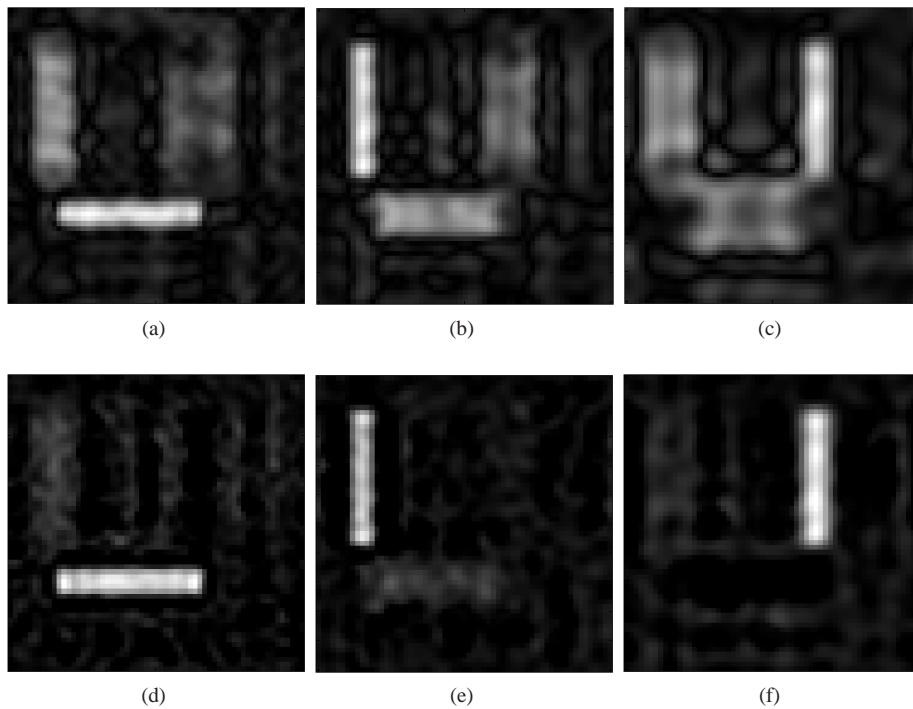


Fig. 9. Reconstructed sections from a hologram with three sections. Fig. 9(a), Fig. 9(b) and Fig. 9(c) show results of sections at  $z_1$ ,  $z_2$  and  $z_3$  by the conventional method. Shown in Fig. 9(d), Fig. 9(e) and Fig. 9(f) are reconstructed sectional images at  $z_1$ ,  $z_2$  and  $z_3$  by the inverse imaging method.

distorts the information of focused element. The distortion is more seriously than it is in the two-section hologram, because there are two sections bringing the defocused noise into the focused section. Even though, the focused element is prominent relatively in corresponding sections. In comparison, those reconstructions using the inverse imaging method are shown in Fig. 9(d), Fig. 9(e) and Fig. 9(f). In the regularized results, the element in each section is distinctly recovered and the defocus noise is effectively suppressed. SNR is measured with regard to the regularization parameter  $\lambda$  and shown in Fig. 10. Regularization parameter affects the image quality of the reconstruction. We can yield similar results in terms of SNR by choosing  $\lambda$  from 15 to 4000. A rather large range of  $\lambda$  demonstrates that the reconstruction is not sensitive to the choice of the regularization parameter.

In summary, compared with existing proposed methods, such as Wiener filter and WDF, our reconstruction is more effective in terms of suppressing noise and recovering multiple sections. The suppression does not depend heavily on the choice of parameters, allowing rather a straightforward implementation. In contrast, the estimation of the power spectrum of the noise in Wiener filter is sensitive to the number of sections. The spectrum of the defocus noise in the multiple-section hologram might overwhelm that of the focused element and cause the filter ineffective. In WDF, the rotation of components to different degrees is limited by the spatial separation of the sectional images and inference inherent in the transform. The rotation determines the separability of components in the space and frequency domains, while multiple

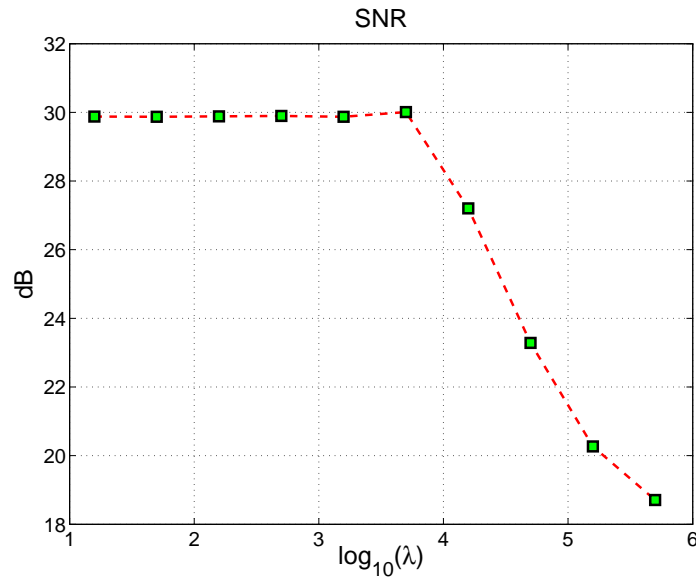


Fig. 10. SNR with regard to the regularization parameter.

sections restrict the degree of the rotation of every section.

## 5. Conclusions

In the reconstruction of sectional images from a hologram generated by OSH, difficulties from the defocus noise and multiple sections make it hard to achieve sectional images in good quality. In the paper, we propose a novel model to reformulate the scanning technique, in which matrix multiplication replaces the convolution operation to express a hologram. The reconstruction is equivalent to solving an ill-posed inverse problem. Then the regularization method is used to yield the reconstructed sections. Our results demonstrate that our method is versatile and can achieve reconstructions with good image quality.

## Acknowledgment

This work was supported in part by the University Research Committee of the University of Hong Kong under Project 10208291.